

Convective Instability Associated with the Eastward-Propagating Rainfall Episodes over Eastern China during the Warm Season

GUIXING CHEN, RYUHEI YOSHIDA, WEIMING SHA, AND TOSHIKI IWASAKI

Department of Geophysics, Graduate School of Science, Tohoku University, Sendai, Japan

HUILING QIN

South China Sea Institute of Oceanology, Chinese Academy of Science, Guangzhou, China

(Manuscript received 25 July 2013, in final form 28 November 2013)

ABSTRACT


Analysis of the latest satellite rainfall and reanalysis datasets from 1998 to 2012 demonstrates that eastward-propagating rainfall episodes, which typically occur in late night and morning, are determinant factors for the rainfall diurnal cycle and climate anomalies over eastern China. The episode growth and propagation are facilitated by an elevated layer of conditionally unstable air in a mesoscale zone at their eastern leading edge. The convective available potential energy (CAPE), despite convection consumption and nocturnal cooling, decreases only from a high value to a moderate one during episode duration. An estimate of the CAPE generation budget suggests that low-level horizontal advection and vertical lifting of the warm moist air can produce sufficient CAPE to balance other stabilization effects, sustaining the mesoscale maximum of convective instability ahead of rainfall episodes. These instability geneses are pronounced at the convection growth stage and linked closely to a mesoscale nocturnal low-level jet. Thus, a proper representation of them in forecast models is essential for improved prediction of the warm-season rainfall.

1. Introduction

Eastward propagation of atmospheric convective systems is a common feature at the eastern lee side of high terrain such as the Tibetan Plateau and the Rockies (Asai et al. 1998; Wang et al. 2004, 2011; Carbone et al. 2002; Jiang et al. 2006). The migrating episodes can last for longer than 12 h and traverse more than 1000 km, indicating an intrinsic predictability of the warm-season rainfall. These episodes are also fixed in diurnal phase and prefer to occur at night. Over eastern China, they help produce a midnight rainfall peak at the plateau foothills and a late night–morning rainfall peak in the lowlands farther east (Xu and Zipser 2011; Wang et al. 2012; Chen et al. 2012). The nocturnal rainfall, distinct from the afternoon rainfall in most inland areas, is

recognized as being an important aspect of regional weather/climate (Yu et al. 2007; Chen et al. 2009a; Yuan et al. 2010). Consequently, a reliable representation of these migratory episodes in numerical models is crucial for improving the prediction of summertime rainfall on both diurnal and seasonal time scales.

A large amount of moisture and convective instability are the key conditions for sustaining the long-lived convective systems. Over eastern China, these conditions can be linked to a low-level moisture transport (Li et al. 2007; Chen et al. 2012; Wang et al. 2012), a reversal of mountain–plain circulation (Bao et al. 2011; Yuan et al. 2012b), a diurnal cycle of monsoon flow (Chen et al. 2009b, 2013), and midlevel cold advection from plateaus to foothills (Chen et al. 2010; Jin et al. 2013). Over the U.S. Great Plains, enhanced convective available potential energy (CAPE) at the northern terminus of the low-level jet (LLJ) also exhibits a strong association with nocturnal organized convection (Tuttle and Davis 2006). A deep layer of moist unstable air greatly supports convection growth at night (Trier et al. 2006), whereas a decayed supply of warm moist air engenders convection dissipation (Gale et al. 2002). As indicated, further studies of the change of moist instability can

 Denotes Open Access content.

Corresponding author address: Guixing Chen, Department of Geophysics, Graduate School of Science, Tohoku University, A519, Physics A Bldg., 6-3, Aoba, Aramaki, Aoba, Sendai, Miyagi 980-8578, Japan.
E-mail: chen@wind.gp.tohoku.ac.jp

DOI: 10.1175/JCLI-D-13-00443.1

improve clarification of how convective systems respond to their environments producing heavy rainfall.

Most previous studies have specifically addressed the synoptic conditions associated with rainfall episodes over eastern China. Because of difficulty in tracking the rainfall footprint and mesoscale weather for lack of fine-resolution data, a detailed picture of the mesoscale environment of rainfall episodes has been unavailable in the past. In particular, the relative roles of various physical processes in regulating convective instability remain to be quantified. Using new-generation satellite rainfall and reanalysis datasets, we make an attempt to examine the meso- α -scale structures of rainfall episodes. We quantitatively assess the CAPE genesis processes to understand what controls the change of convective instability associated with the life cycle of rainfall episodes.

2. Data and methods

For rainfall observation, we use rain estimates (3B42, version 7) from the Tropical Rainfall Measuring Mission (TRMM; Huffman et al. 2007). The 3B42 is a combination of TRMM-calibrated microwave rainfall estimates with infrared rainfall estimates. With multiple microwave sensors at the low Earth orbit, high-quality microwave rainfall estimates can cover a large portion of the tropics surface at any 3-hourly interval (Huffman et al. 2007). The latest version 7 of 3B42 supersedes all previous versions in many aspects; it employs improved gauge analysis for calibration to reduce the land bias particularly over mountainous regions. Compared with ground-based radar, the 3B42 gives an improved capture of the rainfall volume and location of mesoscale convective systems, relative to the other satellite products mainly based on infrared rainfall estimates (Demaria et al. 2011). Over eastern China, the rainfall diurnal cycle and propagation in 3B42 are somewhat consistent with the observed by precipitation radar on board TRMM (Chen et al. 2012). The 3B42 may underestimate some fraction of morning rainfall when compared to rain gauge data. Yuan et al. (2012a) suggested that this underestimate is mainly due to the massive morning light rainfall missed in 3B42, which is more evident in plains than that in mountains. In this study, a criterion of rain rate ($\geq 1 \text{ mm h}^{-1}$) is applied in the detection of rainfall events as in Chen et al. (2013), which helps to mitigate the effect of 3B42 deficiency on diurnal cycle (if there is any).

To depict the atmospheric processes, we use the latest reanalysis product, the European Centre for Medium-Range Weather Forecasts (ECMWF) Interim Reanalysis (ERA-Interim; Dee et al. 2011). ERA-Interim

has a resolution of 6 h at 0.75° longitude–latitude, whereas the 3B42 is available 3-hourly at 0.25° . These high-resolution data enable a capture of the environments of meso- α -scale nocturnal rain systems (with an area size of about $1 \times 10^5 \text{ km}^2$ or a horizontal scale of about 300 km) that are dominant over eastern China (Chen et al. 2012, 2013). Compared with sounding data, ERA-Interim has been shown to represent the wind variations in both daily and diurnal time scales (Chen et al. 2013). Similarly, we check that it also captures well the CAPE variations over eastern China (figure not shown).

To identify rainfall episodes, we use a method derived by Carbone et al. (2002), who defined an episode as clusters of rain systems aligned along a linear axis in the Hovmöller (longitude–time) space. Most parameters in this method are set identically to those in Carbone et al. (2002), except that 3B42 rainfall averaged in 26° – 32°N is used. We focus on the rainy season of May–July when propagating episodes are most active over eastern China (Wang et al. 2004; Chen et al. 2012). During May–July of 1998–2012, there were 337 days with rainfall episodes observed at 105° – 110°E . The rainfall of these episode days (24% of the total days) represents a contribution to the warm-season rainfall budget. For better representativeness, 43 typical episodes are identified using more restrictive criteria (for rainfall amount and resemblance to idealized propagation pattern) in the selection process. We note that rainfall episodes usually grow at late night (0100–0400 LT) and reach maturity in the morning (0700–1000 LT), similar to cloud episodes (Wang et al. 2012). The episodes also have a long duration of more than 12 h, allowing the satellite rainfall and reanalysis data to depict their major stages. The hour with the largest rainfall increase denotes the episode's growth stage and the adjacent hours ($\pm 6 \text{ h}$) denote the initiation and mature stages, respectively. To make a mesoscale composite of episodes, we locate the associated meso- α -scale systems as the rainfall-weighted centers of continuous rainy area precisely (Chen et al. 2013). Then, we artificially shift the observed rainfall and atmospheric variables to the mean locations according to the episode's life cycle.

We use CAPE as a measure of convective instability (Moncrieff and Miller 1976; Emanuel 1994):

$$\text{CAPE} = \int_{p_{\text{lnb}}}^{p_{\text{sl}}} R_d (T_{v_p} - T_{v_e}) d \ln p. \quad (1)$$

Therein, T_{v_p} and T_{v_e} are virtual temperatures of the air parcel and the environment aloft as the air parcel is lifted, following an undilute adiabat, from the source level p_{sl} to the level of neutral buoyancy p_{lnb} . We calculate the CAPE values for the parcels from different

source levels. Based on the deduction reported by Emanuel (1994) and Zhang (2002), the time rate of change of CAPE is given as follows:

$$\frac{\partial \text{CAPE}}{\partial t} = \int_{p_{\text{lnb}}}^{p_{\text{sl}}} R_d \left(\frac{\partial T_{v_p}}{\partial t} - \frac{\partial T_{v_e}}{\partial t} \right) d \ln p$$

$$\approx C_p (T_{v_{\text{sl}}} - T_{v_{\text{lnb}}}) \frac{\partial \ln(\theta_e)}{\partial t} - \frac{\partial}{\partial t} (\phi_{\text{lnb}} - \phi_{\text{sl}}). \quad (2)$$

As indicated, CAPE might change when either T_{v_p} or that of T_{v_e} changes. It also relates to either a change of the air parcel's equivalent potential temperature θ_e or a change of the geopotential thickness of convection layer ($\phi_{\text{lnb}} - \phi_{\text{sl}}$). In this respect, the CAPE generation rates are linked to the boundary layer and free-atmospheric forcings (Zhang 2002, 2003). For greater detail of low-level processes, we expand the local change of θ_e :

$$\frac{\partial \theta_e}{\partial t} = -u \frac{\partial \theta_e}{\partial x} - v \frac{\partial \theta_e}{\partial y} - w \frac{\partial \theta_e}{\partial z} + Q. \quad (3)$$

By combining Eq. (3) with Eq. (2), we can further specify boundary layer forcings as those CAPE generation rates because of horizontal advection, vertical lifting, and external diabatic heating Q . It is noted that over East Asia some long-lived rain systems may occur in the nearly moist neutral stratification, which indicates a release of convective instability (Ninomiya 2004). The impact of convective instability on rain systems can be expressed by the change ratio of instability, more than the instability value itself. Equations (2)–(3) allow us to quantitatively estimate the CAPE change induced by various processes even when they may balance with each other giving a small CAPE.

3. Results

Figure 1a displays the composite rainfall of all 337 episode days. Rainfall appears markedly around 2200 LT at the slope of the Tibetan Plateau ($\sim 104^\circ\text{E}$). It tends to occur in the foothills ($105^\circ\text{--}106^\circ\text{E}$) around 0100 LT, intensifies, and moves eastward during 0100–0400 LT. The episodes bring extensive rainfall farther east, at $108^\circ\text{--}112^\circ\text{E}$, during 0500–1100 LT. The axis of intense rainfall stretches approximately from 106° to 110°E in 6 h, indicating a mean phase speed of about 18 m s^{-1} , which is consistent with the propagation speed of cloud episodes (Wang et al. 2004, 2011). Figure 1a also shows that strong rainfall is recorded at a wide hour range at 110°E , likely due to the various timings of episodes' arrival.

Figure 1b shows regional mean diurnal cycles for elucidating the role of episodes on rainfall budget. The 15-yr-mean rainfall attains a minimum at 1900 LT and

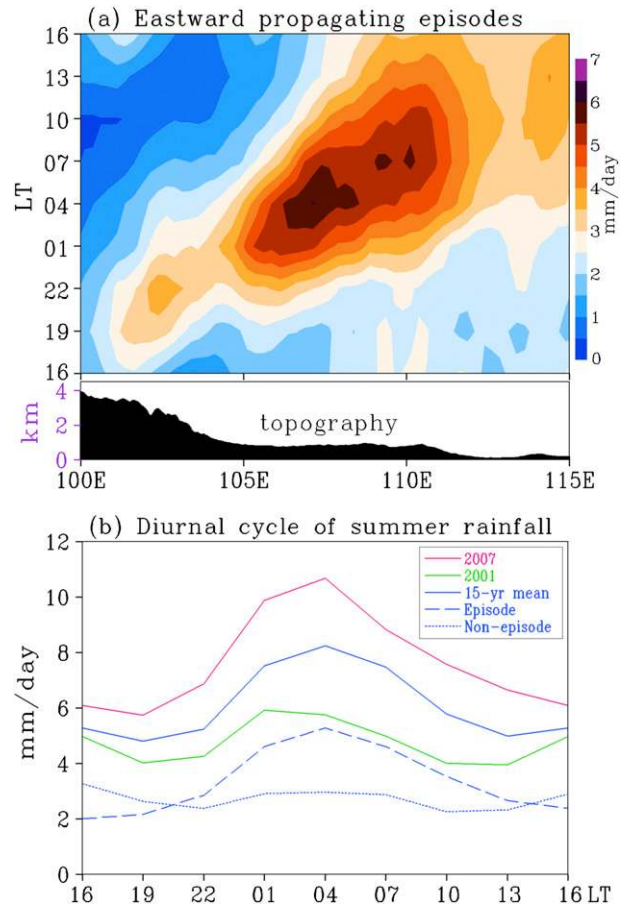


FIG. 1. (a) Hovmöller (longitude–time) diagram of the summer rainfall by eastward-propagating rainfall episodes in the $26^\circ\text{--}32^\circ\text{N}$ zone in 1998–2012. The mean elevation is shown at the bottom. (b) Diurnal cycle of the summer rainfall averaged over eastern China ($26^\circ\text{--}32^\circ\text{N}$, $105^\circ\text{--}110^\circ\text{E}$), estimated for the individual years of 2007 and 2001, the 15-yr mean for 1998–2012, and days with and without episodes.

a maximum at 0400 LT, with a diurnal range of 3.45 mm day^{-1} . The rainfall from episode days accounts for 55% of the warm-season rainfall. Its diurnal cycle is strikingly similar to that of total rainfall. The diurnal range reaches 3.12 mm day^{-1} and explains most of the total diurnal range. In contrast, the rainfall from non-episode days explains 45% of the warm-season rainfall; it displays a very small diurnal range of 0.33 mm day^{-1} . In the wettest summer (2007), diurnal amplitude becomes rather large, with the most enhanced rainfall occurring during late night and morning. This feature corresponds to an active occurrence of rainfall episodes (29 cases) compared to the 15-yr average (22.5 cases per season). In the driest summer (2001), however, only 14 cases of episodes are recorded and contribute a small percentage (42%) of seasonal rainfall. The reduced morning rainfall explains a major part of the

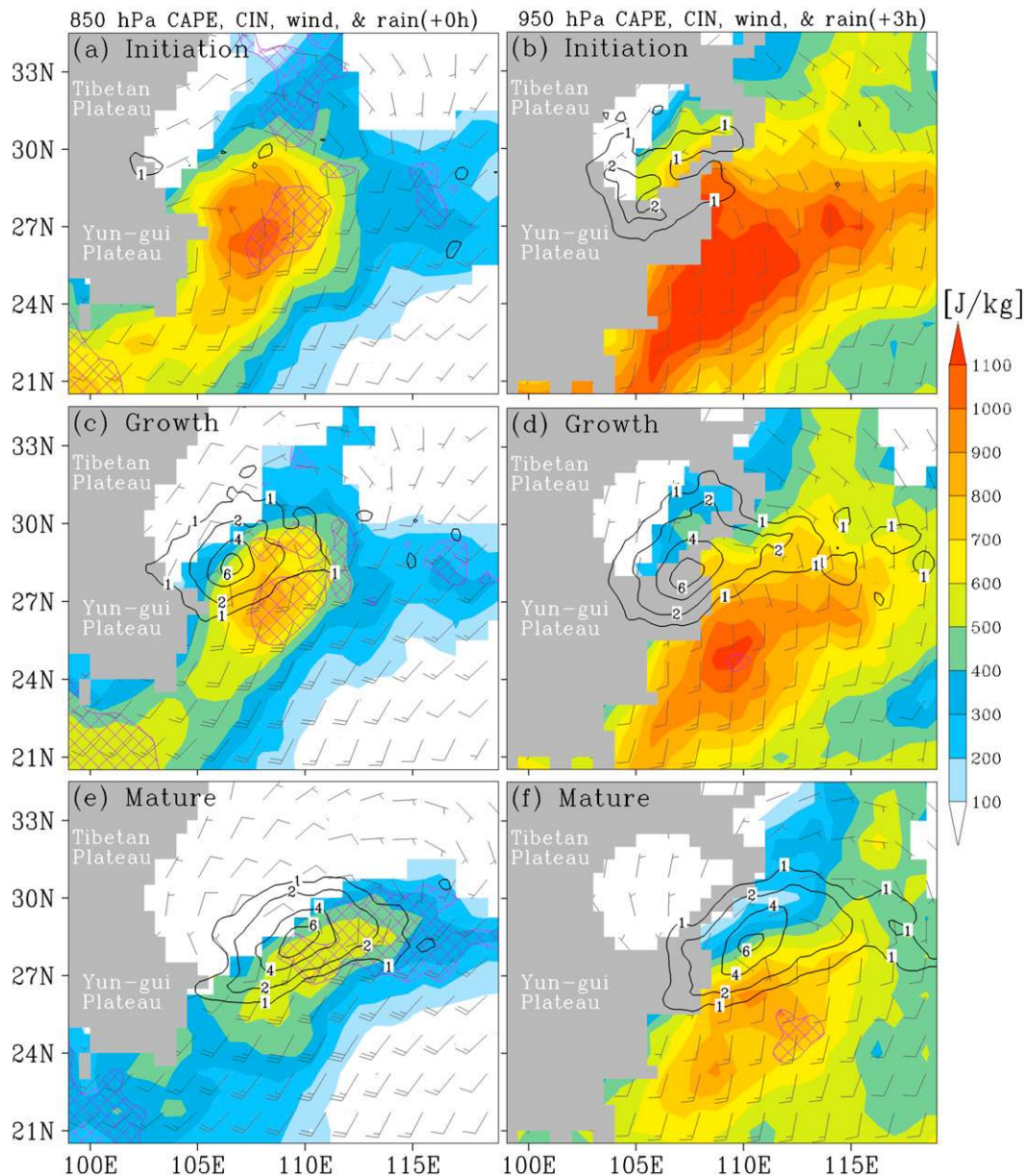


FIG. 2. Composite maps of surface rainfall (contours; mm h^{-1}), low-level horizontal winds (barbs with a full flag for 4 m s^{-1}), CAPE (shaded), and CIN (hatched for $\leq 25 \text{ J kg}^{-1}$) at (a),(b) initiation; (c),(d) growth; and (e),(f) mature stages of the typical episodes. (left) Variables at 850 hPa and 3-h mean rain rate. (right) Variables at 950 hPa and rain rate at next 3-h window. The gray shading in the left and right panels indicates elevations ≥ 1500 and ≥ 750 m, respectively. The method used to make the composite is described in section 2.

rainfall decrease from climate mean. It seems clear from Fig. 1 that eastward-propagating episodes play a key role in the diurnal cycle and anomalies of warm-season rainfall. These prolonged episodes also explain why the nocturnal rainfall by long-duration rain rate exhibits an eastward-delayed diurnal phase over China (Yu et al. 2007), resembling that over the U.S. Great Plains (Jiang et al. 2006).

Figure 2 displays composite maps of 43 typical episodes. The rainfall initiates at the plateau foothills and extends to the Sichuan Basin at 28.5°N , 105°E (Figs. 2a,b). To the southeast of newborn episodes, at 850 hPa there exists a mesoscale zone of high CAPE ($\sim 1000 \text{ J kg}^{-1}$; Fig. 2a). As the low-level winds converge to rainfall episodes, convective systems are supplied with the air mass with high CAPE. At 950 hPa (near surface at most

of eastern China), the high CAPE is observed south of 26°N (Fig. 2b), displaying a warm moist air pool over southern China.

Figures 2c and 2d portray that, at growth stage, rainfall increases in both intensity and area. At 850 hPa, although CAPE declines over most lands, the mesoscale zone of high CAPE ($\sim 800 \text{ J kg}^{-1}$) is maintained at the leading edge of episodes (Fig. 2c), which implies adequate energy for convection growth (Tuttle and Davis 2006). Over there, convection inhibition (CIN) has a small value, and thus, new convective systems are easily generated. As the southerly wind increases to approximately 10 m s^{-1} , the air mass within about 200 km south of the convective zone has a potential to fuel convection in the following 6 h. At 950 hPa, the air mass with high CAPE is centered at 25°N (Fig. 2d). With a relatively large CIN and a low wind speed near surface, this south-located air mass may not directly affect the convective systems. If fueling convection, it should be lifted to a higher layer, where northward transport is faster.

Figure 2e shows that, when episodes become mature, intense rainfall stretches southwest–northeast and is collocated with the pattern of elevated moderate CAPE and small CIN. The CAPE maximum is located near the episode's center. The moisture advection from southern regions comes to decline (figure omitted). Such a decayed supply of external warm moist air is often followed by convection dissipation (Gale et al. 2002) and rainfall intensity decline (Fig. 2f). Unlike the moving CAPE maximum at 850 hPa, the location of high CAPE at 950 hPa is less changed, probably because of a weak wind speed near the surface (Fig. 2f).

Figure 2 highlights that the life cycle of rainfall episodes is characterized by a mesoscale maximum of elevated high CAPE and low CIN. The sustaining instability and weak convective barrier, along with the low-level ascent by strong southwesterly wind, are favorable for the growth of long-lived convection systems (e.g., Trier et al. 2006). As these conditions are established mainly ahead the rainfall episodes, they help to initiate new convection at the east and to support the eastward movement of episodes. With a steady-state model applied to small-shear atmosphere, Moncrieff and Miller (1976) suggest that the convection may propagate at a speed of approximately $0.3\sqrt{\text{CAPE}}$ relative to mid-level winds. As we see a CAPE value of $600\text{--}900 \text{ J kg}^{-1}$ and a midlevel westerly of about 10 m s^{-1} over China, the episode propagation speed of about 18 m s^{-1} seems to be in an acceptable range. Such an influence of instability on convection propagation is also plausible for the rainfall episodes over the U.S. Great Plains (Carbone et al. 2002). In contrast, during the nonpropagating rainfall events that stay near the plateau foothills, the

mesoscale maximum of convective instability and low-level southwesterly wind at the southeastern edge as well as the midlevel westerly are less pronounced (figure not shown).

We proceed to examine the CAPE genesis budget to clarify what controls the change of convective instability. We focus on the sustenance mechanisms of CAPE maximum leading the rainfall episodes. As a major moisture source comes from south, a south–north cross section is made at the eastern edge of episodes for 6 h before their growth stage. Figure 3a shows that CAPE declines by more than 300 J kg^{-1} near the surface at convective zone and in the lower troposphere near 24°N , whereas it decreases by only about 100 J kg^{-1} at 850 hPa near 27°N . The CAPE turns to increase at the updraft layer above 850 hPa near 28.5°N . This corresponds to a deep layer of CAPE tilting upward at the convective zone. Figure 3b shows that the free-tropospheric forcings (nocturnal cooling aloft) generate a small CAPE for most latitudes, except at convective zone where warm advection ahead of mid- to -upper-level troughs might stabilize stratification.

Comparing Figs. 3c and 3a, it is apparent that the CAPE change is mainly attributable to the boundary layer forcings that regulate the moist static energy of air parcels. Figure 3d shows that, among the forcings, horizontal advection can enhance CAPE by $200\text{--}300 \text{ J kg}^{-1}$ at the convective zone and the adjacent southern areas, suggesting that the inflow of warm moist air is effective in yielding CAPE for growing convection. The advection reduces CAPE by about 500 J kg^{-1} in remote southern areas where it transports warm moist air northward. Figure 3e shows that vertical lifting enhances CAPE by $200\text{--}300 \text{ J kg}^{-1}$ at the top of a warm moist air mass, with one maximum at 26°N and another at the convective zone. Moisture upwelling in the boundary layer thus helps to maintain the elevated conditionally unstable layer. Figure 3f shows that the cooling of air parcels tends to reduce CAPE on land. The reduction is greatest near ground at the convective zone, where strong cooling may arise from raindrop fallout.

From Fig. 3, it seems clear that low-level horizontal advection and vertical lifting play a crucial role in generating the convective instability at the leading eastern edge of moist convection. These instability geneses are comparable to, if not greater than, cooling stabilizations, thereby slowing the CAPE depletion and maintaining the CAPE maximum at night. In contrast, at the western rear of rainfall episodes, there observes a large CAPE decrease mainly due to the diabatic cooling (figure not shown). The CAPE genesis pattern, with a positive leading and a negative lagging the episode center, is thought to maintain the west–east gradient of convective

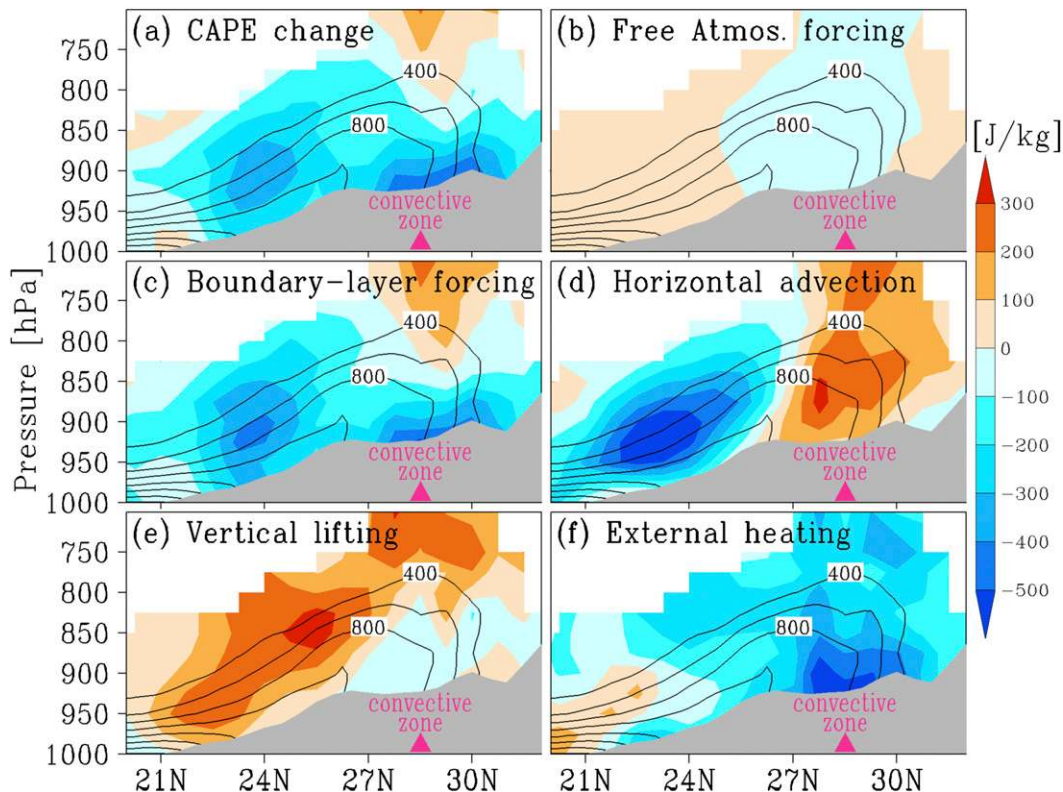


FIG. 3. Latitude–pressure section of (a) the CAPE change and (b)–(f) the CAPE generation rates by various physical processes at the eastern edge of episodes for 6 h from initial to growth stages. Panels correspond to the terms in Eqs. (2) and (3): from Eq. (2), (a) \approx (b) + (c), and from Eq. (3), (c) = (d) + (e) + (f). The section is made at 108.75°E, given that the episodes' centers were shifted to 28.5°N, 106.5°E. The contours show CAPE values at the growth stage. The topography is shaded in gray.

instability and thereby to favor the eastward movement of rainfall episodes.

For more insights into the CAPE genesis, a composite analysis of weather conditions is performed at 850 hPa. From initial to growth stages, both southerly wind and upward motion strengthen at the eastern lee side of plateaus (Figs. 4a–d). Moisture advection/lifting enhances the CAPE generation leading the convective center (Fig. 4c). Low-level convergence becomes strong at the northern terminus of increased wind speed and on the southeastern flank of low pressure (Fig. 4d), which helps organize the air mass of enhanced convective instability into narrow regions favoring the convection growth (Fig. 2c). Such a strong southerly wind has an ageostrophic component and manifests as a mesoscale nocturnal LLJ (Li et al. 2007; Chen et al. 2009b, 2012). Although weather patterns may vary considerably among episodes, the presence of nocturnal LLJ remains persistent, as also noted by Wang et al. (2012). Figure 4d shows that the enhanced southerly originates in southern warm regions and relates to a diurnal cycle of monsoon flow (Chen et al. 2013). It differs somewhat from that over the

U.S. Great Plains, where LLJ-related rising motion is intensified at frontogenetic zones as a response to the thermally direct cross-frontal circulation (Trier et al. 2006). At mature stage, the increased wind speed propagates downstream (Fig. 4f). The wind core is established near the rainfall center, probably because of condensational heating, and strong moisture inflow may play a positive feedback sustaining rainfall systems (Qian et al. 2004). In southern regions, however, the low-level winds are divergent (Fig. 4f), reducing upward motion and CAPE genesis despite some orographic lifting (Fig. 4e). This weakens the external supply of moisture and instability for episodes.

4. Conclusions

Results of this study show that eastward-propagating episodes greatly influence the rainfall diurnal cycle over eastern China. The episodes are active (suppressed) in a wet (dry) year and thus appear responsible for warm-season rainfall anomalies. They are distinctly supported by a mesoscale zone of elevated conditionally unstable

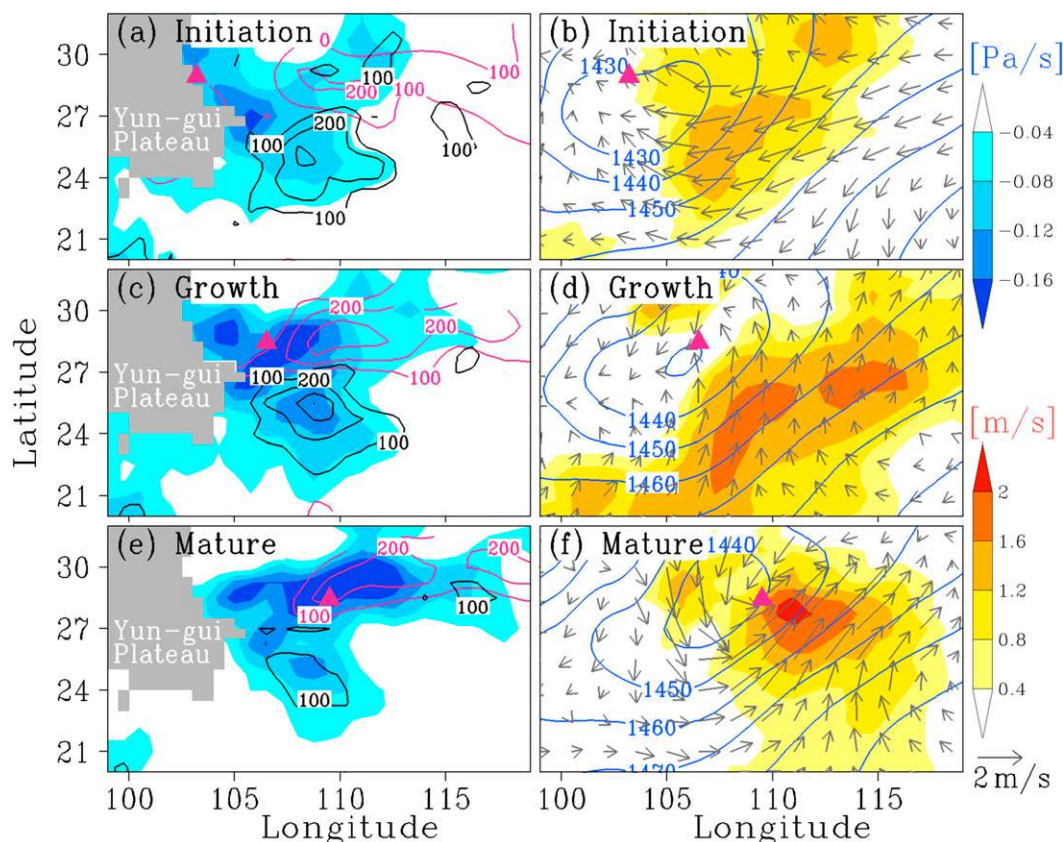


FIG. 4. Composite maps of the CAPE genes and atmospheric conditions at 850 hPa at (a),(b) initiation; (c),(d) growth; and (e),(f) mature stages. (left) Upward motion (blue shading), 6-h CAPE genes by vertical lifting (black contours), and by horizontal advection (red contours). Elevations ≥ 1500 m is shaded in gray. (right) Geopotential height (blue contours; 10 gpm), 6-h increase of wind speed (red shaded), and diurnal component of horizontal winds (vectors). The diurnal component is estimated as the wind deviation from the daily mean. The mean centers of rainfall episodes are marked by triangles.

air, with a large CAPE and a small CIN, at their eastern leading edges. The governing equation of CAPE is used to estimate the instability generation rates of various physics processes. It shows that the CAPE change is mostly due to the boundary layer forcings, while the free-tropospheric forcings have a smaller effect. In particular, both low-level horizontal advection and vertical lifting of the warm moist air can generate CAPE by $200\text{--}300 \text{ J kg}^{-1} (6 \text{ h})^{-1}$. They act to maintain the CAPE maximum against the cooling stabilizations. Specifically, the upwelling of a moisture source from the south helps to sustain the elevated layer of conditionally unstable air, while the moisture transport into the convective zone further yields instability for growing convection. Such processes are strongly regulated by a mesoscale nocturnal LLJ, highlighting the monsoon flow that diurnally strengthens convective instability, more than moisture supply and ascending motion, for supporting the warm-season rainfall systems.

In this composite analysis, we report a strong association between convective instability and nocturnal growth/propagation of rainfall episodes over eastern China, which is similar to that observed over the U.S. Great Plains (e.g., Tuttle and Davis 2006). With a quantitative estimate of physics processes that control the CAPE change, we gain an insight into the nocturnal rainfall and its propagating behavior from the instability aspect. It is recognized that, besides convective instability, the propagating episodes also involve a variety of dynamic factors, including wind shear (Wang et al. 2011, 2012), mountain–plain solenoids (Bao et al. 2011; Jin et al. 2013), cold pool dynamics (Trier et al. 2006; Bao and Zhang 2013), diurnal veering of the low-level winds (G. Chen et al. 2009b, 2012; H. Chen et al. 2010), and/or wavelike mechanisms (Carbone et al. 2002). An estimate of the relative roles of all these factors in regulating propagation speed, although beyond the instability scope of this study, deserves further research in the future.

On the other hand, one meso- α -scale rainfall event usually consists of several individual convective systems at smaller scale. The satellite rainfall and reanalysis data, while presenting the meso- α -scale features of the major stages of episodes, are inadequate to resolve the embedded meso- β -scale systems that have a shorter duration of several hours. Thus, further clarification of the dynamics of propagating episodes may benefit from the observational analyses at higher resolution in time and space.

Most general circulation models with CAPE-based convective schemes show a deficiency in the simulation of nocturnal rainfall episodes (Dai and Trenberth 2004; Jiang et al. 2006). Over eastern China, climate models suffer large biases in rainfall diurnal cycle due to convective parameterization (Yuan et al. 2013). Because CAPE reaches its maximum in the afternoon near the surface due to latent/sensible heat, it is not directly related to nocturnal convection. As nocturnal convection relies heavily on convective instability at an elevated layer, a solution to properly modeling them is the use of a new triggering function for a convective scheme based either on the convection starting level (Lee et al. 2008) or on the CAPE genesis rates that are in phase with nocturnal convection (Zhang 2003). In view of the fact that the moisture conveyor and upwelling greatly influence the elevated convective instability, a proper representation of this linkage in the climate models will serve to improve the prediction of rainfall episodes. Numerical studies at higher resolution are also warranted to provide additional insights into severe flooding and climate anomalies over eastern China and other similar weather regimes.

Acknowledgments. The authors wish to thank three anonymous reviewers for their helpful comments. They also thank the ECMWF for providing the reanalysis dataset and NASA Goddard Space Flight Center for providing the satellite rainfall dataset. This study was partly supported by the Strategic Programs for Innovative Research funded by the Ministry of Education, Culture, Sports, Science and Technology (MEXT) in Japan.

REFERENCES

- Asai, T., S. Ke, and Y. Kodama, 1998: Diurnal variability of cloudiness over East Asia and the western Pacific Ocean as revealed by GMS during the warm season. *J. Meteor. Soc. Japan*, **76**, 675–684.
- Bao, X., and F. Zhang, 2013: Impacts of the mountain–plains solenoid and cold pool dynamics on the diurnal variation of warm-season precipitation over northern China. *Atmos. Chem. Phys.*, **13**, 6965–6982.
- , —, and J. Sun, 2011: Diurnal variations of warm-season precipitation east of the Tibetan Plateau over China. *Mon. Wea. Rev.*, **139**, 2790–2810.
- Carbone, R. E., J. D. Tuttle, D. A. Ahijevych, and S. B. Trier, 2002: Inferences of predictability associated with warm season precipitation episodes. *J. Atmos. Sci.*, **59**, 2033–2056.
- Chen, G., W. Sha, and T. Iwasaki, 2009a: Diurnal variation of precipitation over southeastern China: 1. Spatial distribution and its seasonality. *J. Geophys. Res.*, **114**, D13103, doi:10.1029/2008JD011103.
- , —, and —, 2009b: Diurnal variation of precipitation over southeastern China: 2. Impact of the diurnal monsoon variability. *J. Geophys. Res.*, **114**, D21105, doi:10.1029/2009JD012181.
- , —, —, and K. Ueno, 2012: Diurnal variation of rainfall in the Yangtze River Valley during the spring–summer transition from TRMM measurements. *J. Geophys. Res.*, **117**, D06106, doi:10.1029/2011JD017056.
- , —, M. Sawada, and T. Iwasaki, 2013: Influence of summer monsoon diurnal cycle on moisture transport and precipitation over eastern China. *J. Geophys. Res. Atmos.*, **118**, 3163–3177, doi:10.1002/jgrd.50337.
- Chen, H., R. Yu, J. Li, W. Yuan, and T. Zhou, 2010: Why nocturnal long-duration rainfall presents an eastward-delayed diurnal phase of rainfall down the Yangtze River Valley. *J. Climate*, **23**, 905–917.
- Dai, A., and K. E. Trenberth, 2004: The diurnal cycle and its depiction in the community climate system model. *J. Climate*, **17**, 930–951.
- Dee, D. P., and Coauthors, 2011: The ERA-Interim reanalysis: Configuration and performance of the data assimilation system. *Quart. J. Roy. Meteor. Soc.*, **137**, 553–597.
- Demaria, E. M. C., D. A. Rodriguez, E. E. Ebert, P. Salio, F. Su, and J. B. Valdes, 2011: Evaluation of mesoscale convective systems in South America using multiple satellite products and an object-based approach. *J. Geophys. Res.*, **116**, D08103, doi:10.1029/2010JD015157.
- Emanuel, K., 1994: *Atmospheric Convection*. Oxford University Press, 580 pp.
- Gale, J. J., J. W. A. Gallus, and K. A. Jungbluth, 2002: Toward improved prediction of mesoscale convective system dissipation. *Wea. Forecasting*, **17**, 856–872.
- Huffman, G. J., and Coauthors, 2007: The TRMM Multisatellite Precipitation Analysis (TMPA): Quasi-global, multiyear, combined-sensor precipitation estimates at fine scales. *J. Hydrometeorol.*, **8**, 38–55.
- Jiang, X., N.-C. Lau, and S. A. Klein, 2006: Role of eastward propagating convection systems in the diurnal cycle and seasonal mean of summertime rainfall over the U.S. Great Plains. *Geophys. Res. Lett.*, **33**, L19809, doi:10.1029/2006GL027022.
- Jin, X., T. Wu, and L. Li, 2013: The quasi-stationary feature of nocturnal precipitation in the Sichuan Basin and the role of the Tibetan Plateau. *Climate Dyn.*, **41** (3–4), 977–994.
- Lee, M.-I., S. D. Schubert, M. J. Suarez, J.-K. E. Schemm, H.-L. Pan, J. Han, and S.-H. Yoo, 2008: Role of convection triggers in the simulation of the diurnal cycle of precipitation over the United States Great Plains in a general circulation model. *J. Geophys. Res.*, **113**, D02111, doi:10.1029/2007JD008984.
- Li, Z., T. Takeda, K. Tsuboki, K. Kato, M. Kawashima, and Y. Fujiyoshi, 2007: Nocturnal evolution of cloud clusters over eastern China during the intensive observation periods of GAME/HUBEX in 1998 and 1999. *J. Meteor. Soc. Japan*, **85**, 25–45.
- Moncrieff, M. W., and M. J. Miller, 1976: The dynamics and simulation of tropical cumulonimbus and squall lines. *Quart. J. Roy. Meteor. Soc.*, **102**, 373–394.

- Ninomiya, K., 2004: Large- and mesoscale features of Meiyu-Baiu front associated with intense rainfalls. *East Asian Monsoon*, C.-P. Chang, Ed., World Scientific, 404–435.
- Qian, J., W. Tao, and K. Lau, 2004: Mechanisms for torrential rain associated with the mei-yu development during SCSMEX 1998. *Mon. Wea. Rev.*, **132**, 3–27.
- Trier, S. B., C. A. Davis, D. A. Ahijevych, M. L. Weisman, and G. H. Bryan, 2006: Mechanisms supporting long-lived episodes of propagating nocturnal convection within a 7-day WRF model simulation. *J. Atmos. Sci.*, **63**, 2437–2461.
- Tuttle, J. D., and C. A. Davis, 2006: Corridors of warm season precipitation in the central United States. *Mon. Wea. Rev.*, **134**, 2297–2317.
- Wang, C.-C., G. T.-J. Chen, and R. E. Carbone, 2004: A climatology of warm-season cloud patterns over East Asia based on GMS infrared brightness temperature observations. *Mon. Wea. Rev.*, **132**, 1606–1629.
- , —, and —, 2011: The relationship between statistics of warm-season cloud episodes and synoptic weather regimes over the East Asian continent. *Meteor. Atmos. Phys.*, **112**, 117–124.
- , —, H.-L. Huang, R. E. Carbone, and S.-W. Chang, 2012: Synoptic conditions associated with propagating and non-propagating cloud/rainfall episodes during the warm season over the East Asian continent. *Mon. Wea. Rev.*, **140**, 721–747.
- Xu, W., and E. J. Zipser, 2011: Diurnal variations of precipitation, deep convection, and lightning over and east of the eastern Tibetan Plateau. *J. Climate*, **24**, 448–465.
- Yu, R., Y. Xu, T. Zhou, and J. Li, 2007: Relation between rainfall duration and diurnal variation in the warm season precipitation over central eastern China. *Geophys. Res. Lett.*, **34**, L13703, doi:10.1029/2007GL030315.
- Yuan, W., R. Yu, H. Chen, J. Li, and M. Zhang, 2010: Subseasonal characteristics of diurnal variation in summer monsoon rainfall over central eastern China. *J. Climate*, **23**, 6684–6695.
- , J. Li, H. Chen, and R. Yu, 2012a: Intercomparison of summer rainfall diurnal features between station rain gauge data and TRMM 3B42 product over central eastern China. *Int. J. Climatol.*, **32**, 1690–1696.
- , R. Yu, M. Zhang, W. Lin, H. Chen, and J. Li, 2012b: Regimes of diurnal variation of summer rainfall over subtropical East Asia. *J. Climate*, **25**, 3307–3320.
- , —, —, —, J. Li, and Y. Fu, 2013: Diurnal cycle of summer precipitation over subtropical East Asia in CAM5. *J. Climate*, **26**, 3159–3172.
- Zhang, G. J., 2002: Convective quasi-equilibrium in midlatitude continental environment and its effect on convective parameterization. *J. Geophys. Res.*, **107**, 4220, doi:10.1029/2001JD001005.
- , 2003: Roles of tropospheric and boundary layer forcing in the diurnal cycle of convection in the U.S. southern Great Plains. *Geophys. Res. Lett.*, **30**, 2281, doi:10.1029/2003GL018554.